Pergamon

International Journal of Machine Tools & Manufacture 42 (2002) 791–800

INTERNATIONAL JOURNAL OF
MACHINE TOOLS
& MANUFACTURE
DESIGN, RESEARCH AND APPLICATION

Prediction of cutting force distribution and its influence on dimensional accuracy in peripheral milling

X.-W. Liu, K. Cheng *, D. Webb, X.-C. Luo

School of Engineering, Leeds Metropolitan University, City Campus, Leeds LS1 3HE, UK

Received 23 October 2001; accepted 24 January 2002

Abstract

Cutting force has a significant influence on the dimensional accuracy due to tool and workpiece deflection in peripheral milling. In this paper, the authors present an improved theoretical dynamic cutting force model for peripheral milling, which includes the size effect of undeformed chip thickness, the influence of the effective rake angle and the chip flow angle. The cutting force coefficients in the model were calibrated with the cutting forces measured by Yucesan [18] in tests on a titanium alloy, and the model was proved to be more accurate than the previous models. Based on the model, a few case studies are presented to investigate the cutting force distribution in cutting tests of the titanium alloy. The simulation results indicate that the cutting force distribution in the cut-in process has a significant influence on the dimensional accuracy of the finished part. Suggestions about how to select the cutter and the cutting parameters were given to get an ideal cutting force distribution, so as to reduce the machining error, meanwhile keeping a high productivity.

Keywords: Cutting force; Distribution; Dimensional accuracy; Peripheral milling

1. Introduction

Peripheral milling is widely used in a variety of industries such as automotive, aerospace, textile machinery and other manufacturing industries, where 2D contour parts, i.e., engine components, cams, etc., are milled using helical end mills. In recent years, due to the need for improving the quality of parts, there has been a push toward decreasing the machining errors in peripheral milling. These errors derive from the machine tools, the cutters, the NC programming and the machining process. The errors of the machining process generated in peripheral milling originate from a number of sources, such as cutting force, tool wear, friction, tool run-out, and chatter vibration. Of these, the machining error due to cutting force is one of the major problems for precision machining.

The machining error due to cutting force originates from tool deflection and workpiece deflection. In order to investigate the influence of cutting force on machining error, not only accurate cutting force but also the dynamic cutting force distribution should be evaluated. For the cutting force prediction, several models based on theoretical assumptions and experimental observations have been developed and reviewed by Smith and Tlusty [13]. A few enhanced cutting force models have been developed in the last decade [1,4–7,9–11,18].

The influence of cutter static deflection due to cutting force on the machining error is investigated by Kline [8], and Sutherland and DeVor [14]. The machining error was predicted using cantilever beam theory for the cutter deflection and finite element method for the workpiece deflection. Cantilever beam theory was also used by Babin [3] in predicting the topography of wall surfaces produced by end mills. In these references, however, the dynamics in the tool/workpiece system was neglected.

The influence of the tool/workpiece system dynamics on surface generation was investigated by Montgomery [10]. The kinematics of the cutter and workpiece vibrations was modelled. Zhang [19,20] introduced the effect of random vibrations on the surface roughness in turning. These vibrations were shown to occur due to the random variation in the micro-hardness of the workpiece material. Elbestawi [6] and Ismail [7] presented a mech-

* Corresponding author.
E-mail address: k.cheng@lmu.ac.uk (K. Cheng).

0890-6955/02/$ - see front matter
PII: S0890-6955(02)00016-0

Nomenclature

Ω	radial immersion angle
α_e	effective rake angle
α_{e0}	initial effective rake angle
α_r	radial rake angle
β	helix angle of end mill
β_s	inclination angle of cut stripe
γ	gap angle between the cut-in process of two flutes
θ	tool rotation angle
θ_m	pitch angle of end mill with m flutes
φ	helix lag angle
φ_s,φ_e	helix lag angular locations of the starting and ending points of contact
φ_i	position angle of a point on the cutting edge of the ith helical flute
ψ	axial immersion angle of a tooth within b_a
ω	spindle rotation angle speed
dF_{ti},dF_{ri}	differential cutting force components of the ith helical flute in tangential and radial direction
dF_{ix},dF_{iy}	differential cutting force components of the ith helical flute in x and y direction
F_{ix},F_{iy}	total cutting force components of the ith helical flute in x and y direction
F_x,F_y	total cutting force components in x and y direction
K_s	tangential cutting force coefficient
R	tool radius
V	cutting speed
b_a	axial depth of cut (peripheral milling)
c	cutting force ratio
d	radial depth of cut (peripheral milling)
f_t	feed per tooth per revolution
m	number of cutter flutes
n	spindle rotation speed (rpm)
t_{ime}	time
t	undeformed chip thickness
$t_i(\varphi_i)$	undeformed chip thickness of the ith tooth in angle position φ_i
t_0	initial undeformed chip thickness
u_0	initial total cutting energy per unit volume

anistic model for surface generation in peripheral milling, which includes the effects of cutter vibrations, run out and flank wear. In all of the above works, there is a lack of a theoretical dynamics model that includes the size effect of undeformed chip thickness and the influence of the effective rake face. Moreover, a practical guidance for reasonable selection of cutter and cutting parameters was not presented to get an ideal dynamic cutting force distribution, so as to improve the dimensional accuracy and surface roughness, meanwhile keeping a high productivity.

The machining error is not proportional directly to the tool and workpiece deflection due to cutting force. Smith and Tlusty [13] illustrated the relationship between the deflection and the error on the machined surface. For simplicity, a milling cutter with straight teeth is considered as shown in Fig. 1. In this case, the deflection will be taken as simply proportional to the instantaneous cutting force rather than the average cutting force. In part (a) of the figure, the radial depth of cut is such that only one tooth is engaged in cutting. This tooth itself is not experiencing any force at the cut-in point A (chip thickness is 0), and there will be no error in location of the surface. In part (b) and (c), although the tooth at point A experiences no force, the forces acting on teeth 2 and 3 will cause a deflection of the cutter which is imprinted by the tooth at A on the surface. This phenomenon demonstrates the importance of the dynamic cutting force distribution to the machining error and that only the dynamic cutting force in the cut-in process of each tooth has influence on the error.

In this paper, an improved theoretical dynamic cutting force model of peripheral milling is presented in Section 2 and an estimation of the cutting force coefficients from previously measured forces in peripheral milling of a titanium alloy is given in Section 3. Predicted cutting forces for the peripheral milling of the titanium alloy from a serious of simulations are presented in Section

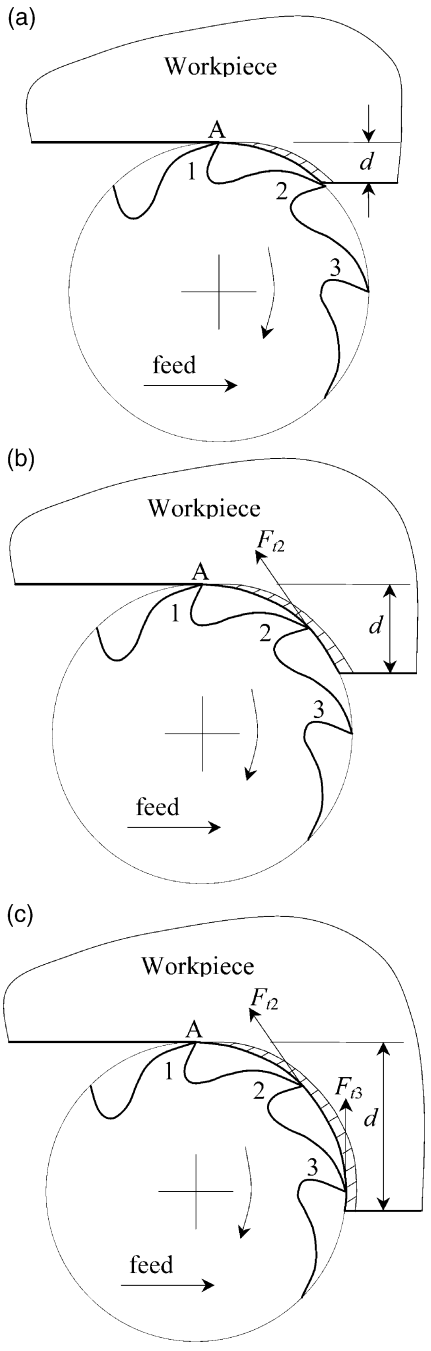

Fig. 1. Milling with various radial immersions. (a) One tooth in cutting; (b) two teeth in cutting; (c) three teeth in cutting.

4. In order to get an ideal dynamic cutting force distribution so as to improve the dimensional accuracy and surface roughness while keeping a high productivity, a practical guidance for reasonable selection of cutter and cutting parameters is given in Section 5.

2. An improved dynamic cutting force model

Among all the cutting force models of peripheral milling, the models presented by Tlusty [15–17], which are formulated from the orthogonal cutting theory [12], are the most essential, and were given in the form of differential tangential and radial cutting forces:

$$dF_t = K_s t(\varphi) dz, \quad (1)$$

$$dF_r = c dF_t, \quad (2)$$

where K_s is the unknown cutting force coefficient, $t(\varphi)$ is the undeformed chip thickness of the tooth element at the helix lag angle position φ, dz is the width of cut, and c is the cutting force ratio. Elbestawi [6], Ismail [7], Kolarits [9] and Montgomery [10] presented their cutting force models which were also originated from the fundamental principle. But in their models, the size effect of undeformed chip thickness and the influence of the effective rake angle, which have significant influence on the cutting forces, were not considered. Based on the orthogonal and oblique cutting principles [12], the authors presented an improved dynamic cutting force model which included the size effect of undeformed chip thickness, the influence of the effective rake angle and the chip flow angle.

Figure 2 shows the helical flute edge geometry of an end mill and the cutting forces acting on a tooth in a section perpendicular to the cutter axis in peripheral milling. The cutting forces acting on the helical flute's rake face are dependent on the undeformed chip thick-

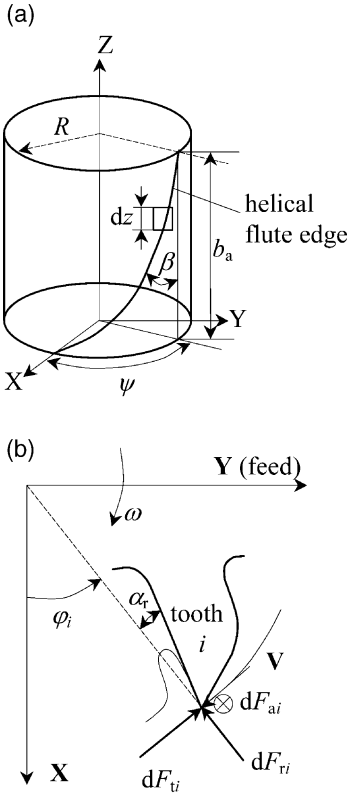

Fig. 2. Cutting force model of peripheral milling. (a) Helical flute edge geometry. (b) Differential tangential and radial forces.

ness, and the differential tangential and radial cutting forces of the tooth have the form:

$$dF_{ti}(\varphi_i) = K_s t_i(\varphi_i) R\cot\beta d\varphi_i, \quad (3)$$

$$dF_{ri}(\varphi_i) = c dF_{ti}(\varphi_i), \quad (4)$$

where K_s is the tangential cutting force coefficient, which has the same meaning as the total energy per unit volume [12], R is the cutter radius, β is the helix angle of the cutter, φ_i is the position angle of a point on the cutting edge of the ith helical flute, c is the force ratio, and $t_i(\varphi_i)$ is the undeformed chip thickness of the tooth element.

Considering the size effect of undeformed chip thickness and the influence of effective rake angle [12], gives

$$K_s = u_0\left(1-\frac{\alpha_e-\alpha_{e0}}{100}\right)\left(\frac{t_0}{t_i(\varphi_i)}\right)^{0.2}, \quad (5)$$

where u_0 is the initial total cutting energy per unit volume, t_0 is the initial undeformed chip thickness, α_{e0} (in degrees) is the initial effective rake angle, and α_e (in degrees) is the effective rake face, which is determined by [12]

$$\sin\alpha_e = \sin\beta\sin\eta_c + \cos\eta_c\cos\beta\sin\alpha_n, \quad (6)$$

where η_c is the chip flow angle and is determined by [2]

$$\tan\eta_c = \tan\beta\cos\alpha_n, \quad (7)$$

and α_n is the normal rake angle and determined by [12]

$$\tan\alpha_n = \tan\alpha_r\cos\beta, \quad (8)$$

where α_r is the radial rake angle.

According to the kinematics of milling, the undeformed chip thickness removed by a point on the ith helical flute can be calculated as follows [12].

For down milling, as shown in Fig. 3(a):

$$t_i(\varphi_i) = \begin{cases} f_t\sin(\varphi_i) & \text{if } 0\le\varphi_i\le\Omega \\ 0 & \text{else} \end{cases}. \quad (9)$$

For up milling, as shown in Fig. 3(b):

$$t_i(\varphi_i) = \begin{cases} f_t\sin(-\varphi_i) & \text{if } -\Omega\le\varphi_i\le 0 \\ 0 & \text{else} \end{cases}, \quad (10)$$

where Ω is the cutter radial immersion angle within the radial depth of cut and

$$\Omega = \arccos\left(1-\frac{d}{R}\right), \quad (11)$$

and the position angle is determined by

$$\varphi_i = \varphi + \theta + (i-1)\frac{2\pi}{m} \qquad (1\le i\le m, 0\le\varphi\le\psi), \quad (12)$$

where

$$\theta = -\omega t_{ime} \quad (13)$$

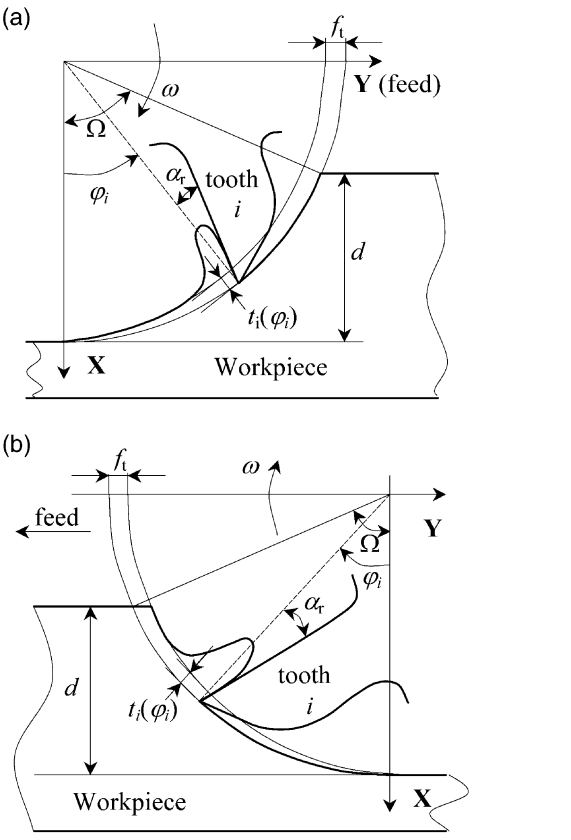

Fig. 3. Peripheral milling method. (a) Down milling. (b) Up milling.

is the instantaneous rotation angle of the flute tip from the x-axis, φ is the helix lag angle, m is the flute number of the cutter, ω is the angular velocity of the spindle, and

$$\psi = \frac{b_a\tan\beta}{R} \quad (14)$$

is the axial immersion angle of a tooth within the axial depth of cut b_a.

Figure 4 shows the relationship of the angles for up

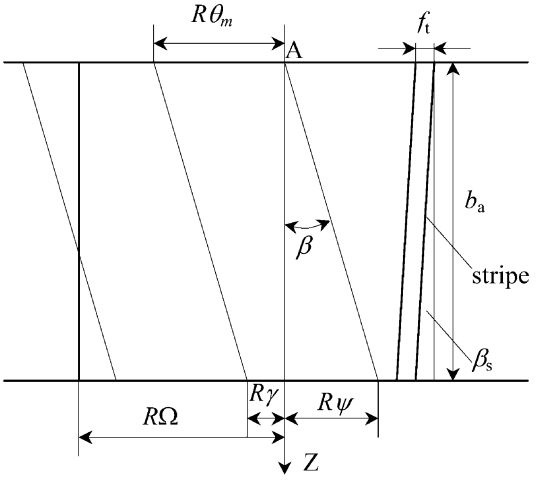

Fig. 4. Relationship of the angles for up milling

milling, where $\theta_m = 2\pi/m$ is the pitch angle of the end mill with m flutes, $\gamma = \theta_m - \psi$ is the gap angle between the cut-in process of two flutes, β_s is the inclination angle of the cut stripe on the machined surface,

$$\tan\beta_s = \frac{f_t m}{2\pi R}\tan\beta. \tag{15}$$

If $\gamma < 0$, there may be two or more flutes in the cut-in process simultaneously. If $\Omega > \theta_m - \psi$, there will be at least one flute engaged in cutting.

To develop the total force applied on the whole cutter, the differential forces are resolved into the feed (y) and normal (x) directions, and Eq. (3) and Eq. (4) become

$$\begin{cases} dF_{tix} = -K_s t_i(\varphi_i) R\cot\beta \sin\varphi_i d\varphi \\ dF_{tiy} = K_s t_i(\varphi_i) R\cot\beta \cos\varphi_i d\varphi \end{cases} \tag{16}$$

$$\begin{cases} dF_{rix} = -cK_s t_i(\varphi_i) R\cot\beta \cos\varphi_i d\varphi \\ dF_{riy} = -cK_s t_i(\varphi_i) R\cot\beta \sin\varphi_i d\varphi \end{cases} \tag{17}$$

Summing these two equations gives the differential forces in x and y as

$$\begin{cases} dF_{ix} = -K_s t_i(\varphi_i) R\cot\beta(\sin\varphi_i + c\cos\varphi_i) d\varphi \\ dF_{iy} = K_s t_i(\varphi_i) R\cot\beta(\cos\varphi_i - c\sin\varphi_i) d\varphi \end{cases} \tag{18}$$

Letting

$$u' = u_0\left(1 - \frac{\alpha_e - \alpha_{e0}}{100}\right)\left(\frac{t_0}{f_t}\right)^{0.2}, \tag{19}$$

and considering the difference between the down milling and up milling, after a few simple substitutions, we can rewrite Eq. (18) as

(a) For down milling:

$$\begin{cases} dF_{ix} = -u' f_t R\cot\beta(\sin^{1.8}\varphi_i + c\sin^{0.8}\varphi_i\cos\varphi_i) d\varphi_i \\ dF_{iy} = u' f_t R\cot\beta(\sin^{0.8}\varphi_i\cos\varphi_i - c\sin^{1.8}\varphi_i) d\varphi_i \end{cases}$$

$$\left(\varphi_i = \varphi - \omega t_{ime} + (i-1)\frac{2\pi}{m} 0 \le \varphi_i \le \Omega\right) \tag{20}$$

(b) For up milling:

$$\begin{cases} dF_{ix} = -u' f_t R\cot\beta[\sin^{1.8}(\xi_i) - c\sin^{0.8}(\xi_i)\cos\xi_i] d\xi_i \\ dF_{iy} = -u' f_t R\cot\beta[\sin^{0.8}(\xi_i)\cos\xi_i + c\sin^{1.8}(\xi_i)] d\xi_i \end{cases}$$

$$\left(\xi_i = -\varphi + \omega t_{ime} - (i-1)\frac{2\pi}{m} 0 \le \xi_i \le \Omega\right) \tag{21}$$

where ($1 \le i \le m$, $0 \le \varphi \le \psi$).

The total cutting force applied on the whole cutting edge is given by

$$\begin{cases} F_{ix} = \int_{\varphi_s}^{\varphi_e} dF_{ix} d\varphi_i \\ F_{iy} = \int_{\varphi_s}^{\varphi_e} dF_{iy} d\varphi_i \end{cases} \text{or} \begin{cases} F_{ix} = \int_{\xi_s}^{\xi_e} dF_{ix} d\xi_i \\ F_{iy} = \int_{\xi_s}^{\xi_e} dF_{iy} d\xi_i \end{cases}, \tag{22}$$

where φ_s (ξ_s) and φ_e (ξ_e) are the lag angular locations of the start and end points of contact of the cutting edge, and are defined in the following kinematics analysis.

(a) For down milling:

Because $0 \le \varphi \le \psi$, $\varphi_i = \varphi - \omega t_{ime} + (i-1)\frac{2\pi}{m}$ and $0 \le \varphi_i \le \Omega$ gives the extreme values of the parametric angle φ_i as

$$\varphi_s = \max(0, -\omega t_{ime} + (i-1)\frac{2\pi}{m}), \tag{23}$$

$$\varphi_e = \min(\Omega, \psi - \omega t_{ime} + (i-1)\frac{2\pi}{m}). \tag{24}$$

(b) For up milling:

Also, $\xi_i = -\varphi + \omega t_{ime} - (i-1)\frac{2\pi}{m}$ and $0 \le \xi_i \le \Omega$ gives the extreme values of the parametric angle ξ_i as

$$\xi_s = \max(0, -\psi + \omega t_{ime} - (i-1)\frac{2\pi}{m}), \tag{25}$$

$$\xi_e = \min(\Omega, \omega t_{ime} - (i-1)\frac{2\pi}{m}). \tag{26}$$

Integrating between the extreme values of the parametric angle φ_s (ξ_s) and φ_e (ξ_e) gives the total cutting force applied on the ith tooth.

For Eq. (20) and Eq. (21) it is impossible to calculate the integrals analytically. However we can approximate the definite integrals with numerical integration.

Summing up the cutting forces acting on all the m helical flutes gives the total force applied on the whole cutter

$$\begin{cases} F_x = \sum_{i=1}^{m} F_{ix} \\ F_y = \sum_{i=1}^{m} F_{iy} \end{cases}. \tag{27}$$

3. Estimation of cutting force coefficients

In Eq. (20) and Eq. (21), the following two coefficients have to be estimated by experiment:

1) u_0, the initial total cutting energy per unit volume, under the initial cutting condition $\alpha_{e0} = 0°$ and $t_0 =$ 0.25mm [12], and

2) c, the cutting force ratio.

u_0 is dependent on workpiece material, cutter material, cutting edge radius, friction characteristics between the workpiece and the cutter (no cutting fluid, continuous chip and no built-up edge are assumed). The ratio c is

about 0.3 [7,15–17] ~ 0.5 [12] and depends mainly on the cutter geometry.

In order to obtain values for the coefficients, some previously measured cutting forces are considered. Yucesan and Altintas [18] have presented a detailed description of their experimentally measured cutting forces in the peripheral milling of a titanium alloy. These experimental results were used to verify a different cutting force model, and it is appropriate to use them to verify our improved cutting force model.

For consistency, we chose the same cutter, workpiece material and cutting conditions (for our simulation) as in the cutting tests conducted by Yucesan and Altintas. These are as follows. Cutter: a single-fluted carbide end mill with a helix angle $\beta = 30°$, a rake angle $\alpha_r = 12°$ and a diameter of 19.06mm. The material properties of the carbide cutter: 90% WC, 10% Co, hardness 92 Rockwell. The material properties of the titanium alloy: 6% Al, 4% V, Young's modulus = 110 GPa, Poisson's ratio = 0.34, tensile strength = 900 Mpa. Cutting parameters: axial depth of cut $b_a = 7.62$mm, radial depth of cut $d = 19.06$mm (slotting), $\psi = 26.45°$, $\Omega = \pi$, spindle rotation speed $n = 500$rpm (cutting speed $V = 498.99$mm/s), with a feed rate ranging from 0.0127 mm/tooth to 0.2030 mm/tooth. The cutting forces measured by Yucesan and Altintas [18] are shown in Fig. 5.

We also assume the conditions presented by Shaw [12]: i.e., that the initial total cutting energy per unit volume $u_0 = 3.51 \times 10^9 \text{J/m}^3$, the initial effective rake angle $\alpha_{e0} = 0°$, the initial undeformed chip thickness $t_0 = 0.25$mm, and the cutting force ratio $c = 0.5$. With these assumed values the instantaneous predicted forces were found to have the same shape as shown in Fig. 5, but with different amplitudes. Adjusting the initial total cutting energy per unit volume and the cutting force ratio to $u_0 = 2.0 \times 10^9 \text{J/m}^3$, $c = 0.45$, the instantaneous predicted forces shown in Fig. 6 are obtained. Comparing these results to the measured cutting forces illustrated in Fig. 5, it is found that there is very good agreement.

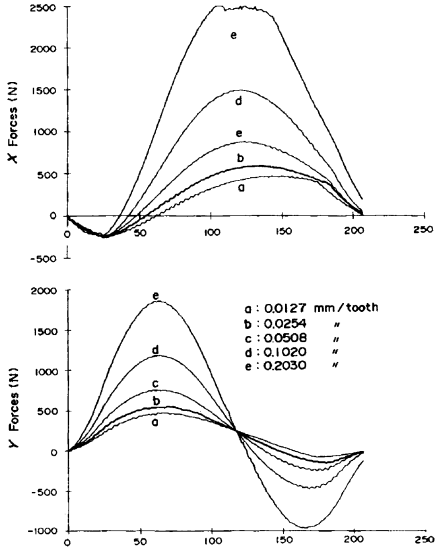

Fig. 5. Measured cutting forces at various feed rates

From Fig. 6 it can be seen that when the feed rate is larger than 0.0254 mm/tooth the predicted cutting forces are very good approximations to the measured cutting forces, and the improved dynamic cutting force model can be used to predict the cutting forces accurately. However, when the feed rate is smaller than 0.0254 mm/tooth, the predicted cutting forces are smaller than the measured values. This result reveals that when the feed rate is far smaller than the radius of the cutting edge, the ploughing force is dominant and the cutting force model must be modified.

4. Prediction of cutting force distribution

From Fig. 3 it can be seen that the tool deflection due to the cutting force component in x has a direct influence on the dimensional accuracy of the machined surface and the one in y has almost no influence on the machining error. For up milling, only the tool deflection during the cut-in process of each tooth will be imprinted directly on the machined surface. So we will concentrate the distribution of F_x during the cut-in process of each tooth in this section.

A series of cutting simulations on the titanium alloy were carried out for tribe- and four-fluted carbide end mills (with a common helix angle of $\beta = 30°$ and a diameter of 19.06mm) at a constant spindle rotation speed of 500rpm. (The cutting speed is constant at $V = 498.99$mm/s).

Figure 7 shows the instantaneous predicted cutting forces for a flute number $m = 4$, a feed rate $f_t = 0.203$ mm/tooth, an axial depth of cut $b_a = 5.08$mm ($\psi = 17.63°$), and a radial depth of cut $d = 9.525$mm ($\Omega = 89.97°$). The gap angle γ between the cut-in process of two flutes is 72.37°, and there is only one tooth engaged in the cut-in process simultaneously. The variation in F_x shows that when the cut-in process of each tooth starts (as the previous tooth cut-out), F_x is 1450 N; and when the cut-in process ends (i.e., the cutter rotation angle = ψ), F_x changes to –80N. This force variation will greatly influence the surface form accuracy of the finished part.

Figure 8 shows predicted values of cutting force for the same condition but for a flute number $m = 3$. As $\Omega < \theta_m - \psi$, there is a gap between the cut-in of one tooth and the cut-out of the previous tooth. The variation in F_x shows that during the cut-in process of each tooth, F_x has small negative values, changing from 0 to –105N. The force variation will have a much smaller influence on the surface form accuracy of the finished part. This result implies the possibility of reducing the surface form error due to tool deflection through carefully selecting

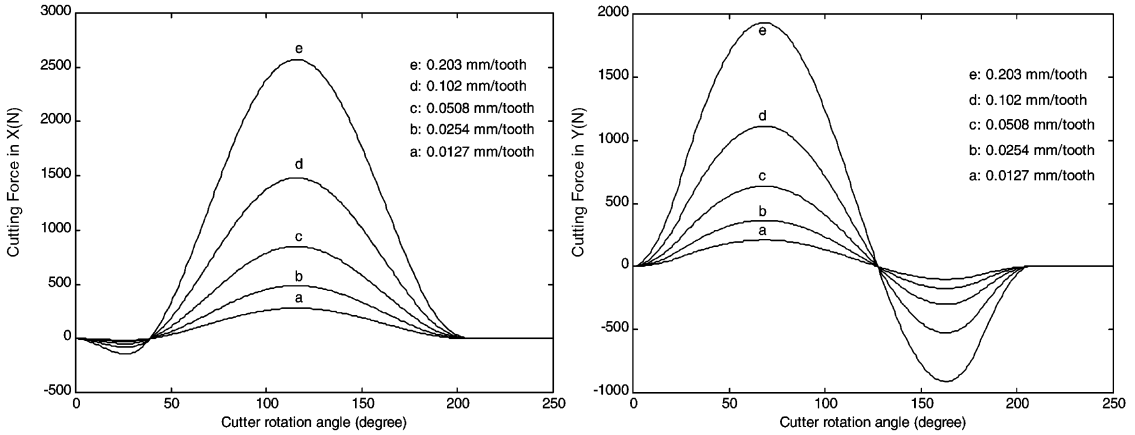

Fig. 6. Predicted cutting forces for a full immersion milling test ($m = 1$, $\alpha_r = 12°$, $b_a = 7.62$mm, $d = 19.06$mm, $\psi = 26.45°$, $u_0 = 2 \times 10^9 J/m^3$)

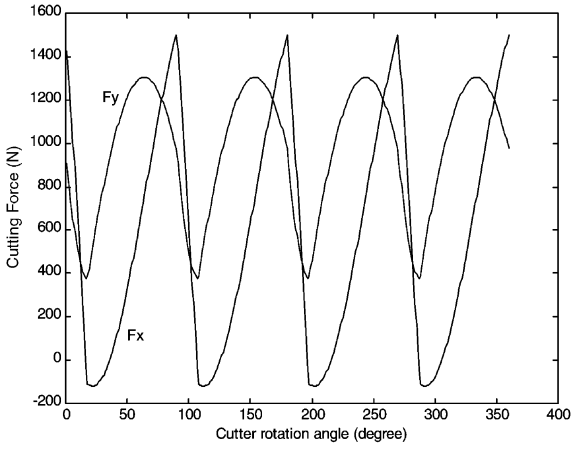

Fig. 7. Predicted cutting forces distribution for a half immersion up milling test ($m = 4$, $f_t = 0.203$mm/tooth, $\alpha_r = 12°$, $b_a = 5.08$mm, $d = 9.525$mm)

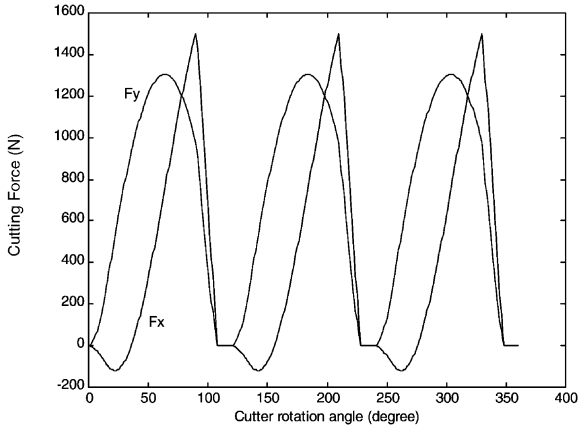

Fig. 8. Predicted cutting forces distribution for a half immersion up milling test ($m = 3$)

the flute number of the cutter. However, this cutting force distribution is not continuous and has a negative influence on the surface form accuracy of the finished part.

Figure 9 shows the predicted cutting forces when the rake angle α_r changes. The only difference is the amplitude of the cutting forces. From these distributions it can be seen that the influence of the rake angle on the cutting force is very obvious.

Figure 10 shows the predicted cutting forces when the feed rate f_t changes. It is worth noticing that when $f_t = 0.102$mm/tooth, the maximum value of F_x is greater than the half maximum value as $f_t = 0.203$mm/tooth, due to the size effect of undeformed chip thickness.

Figure 11 shows the influence of the radial depth of cut on the cutting forces distribution. A very interesting fact is that during the cut-in process of each tooth, when the radial depth of cut changes, the F_x changes significantly. When $d = 6.8$mm, the variation in F_x shows that during the cut-in process of each tooth, F_x has small absolute values, changing from 39 N to –56 N. The force variation will have a much smaller influence on the surface form accuracy of the finished part. And in this case, $\Omega = 73.35° > \theta_m - \psi = 72.37°$, there is a minimum of one tooth engaged in cutting and the cutting force distribution is continuous. This result implies the possibility of reducing the machining error due to tool deflection by carefully selecting the radial depth of cut.

Figure 12 shows an improved cutting forces distribution, where F_x changes from 56 N to –56N during the cut-in process of each tooth. In the test, $d = 6.87$mm, $\Omega = 73.79° > \theta_m - \psi = 72.37°$, and the cutting force distribution is more continuous than in the case of $d = 6.8$mm.

If the radial and axial depth of cut must be kept in variance, we can select a suitable cutter so as to obtain an ideal cutting force distribution. Figure 13 shows the influence of the number of cutter flutes on the cutting

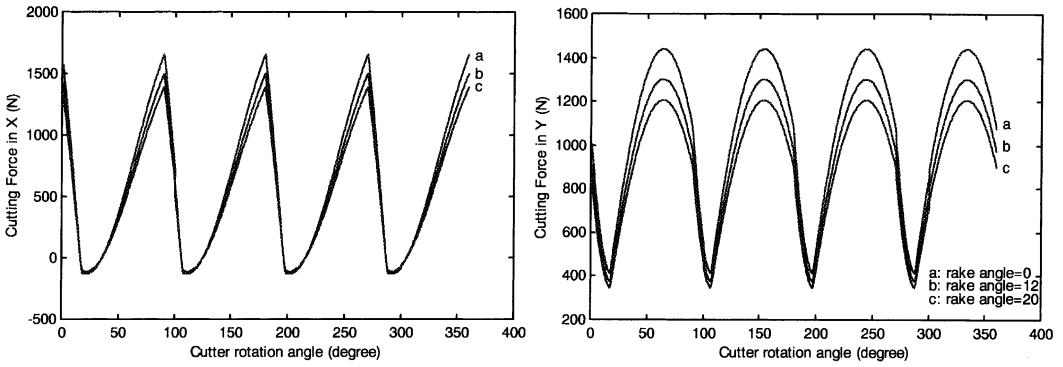

Fig. 9. Influence of rake angle on the cutting forces ($m = 4$, $f_t = 0.203$mm/tooth, $b_a = 5.08$mm, $d = 9.525$mm) (a: $\alpha_r = 0°$, b: $\alpha_r = 12°$, c: $\alpha_r = 20°$)

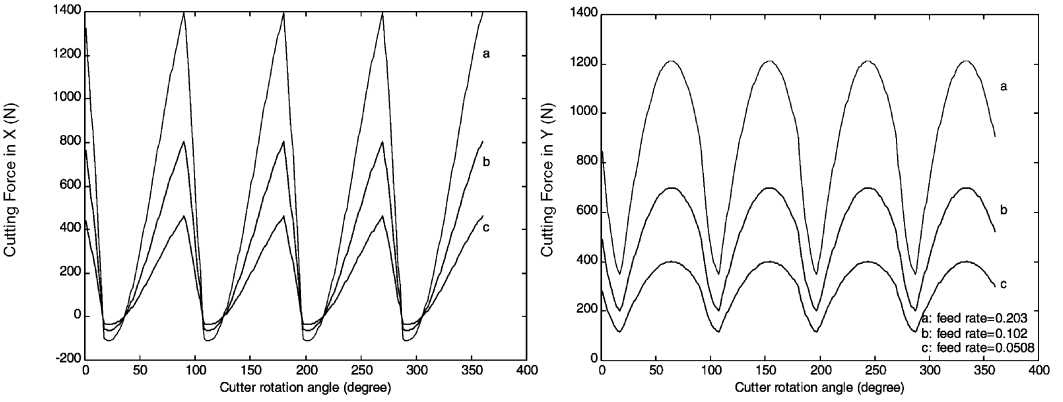

Fig. 10. Influence of feed rate on the cutting forces ($m = 4$, $\alpha_r = 20°$, $b_a = 5.08$mm, $d = 9.525$mm) (a: $f_t = 0.203$mm/tooth, b: $f_t = 0.102$ mm/tooth, c: $f_t = 0.0508$mm/tooth)

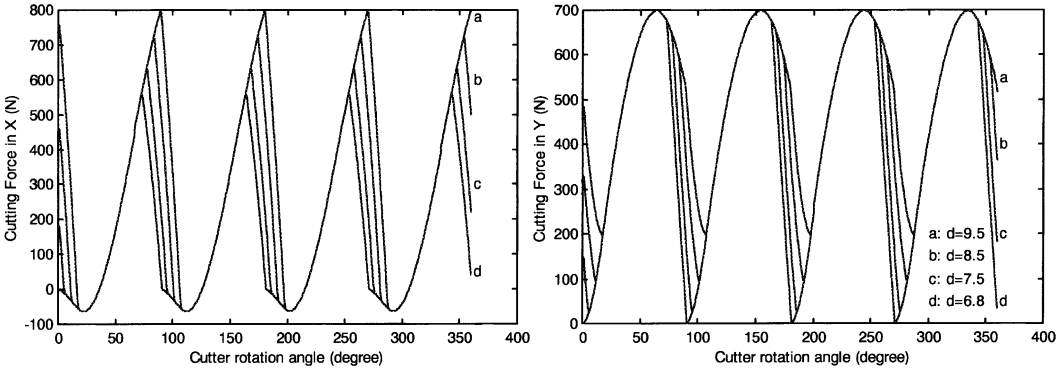

Fig. 11. Influence of radial depth of cut on the cutting forces distribution ($m = 4$, $\alpha_r = 20°$, $b_a = 5.08$mm, $f_t = 0.102$mm/tooth) (a: $d = 9.5$mm, b: $d = 8.5$mm, c: $d = 7.5$mm, d: $d = 6.8$mm)

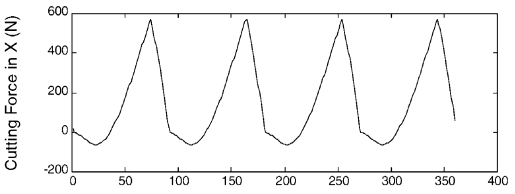

Fig. 12. An idea cutting forces distribution ($m = 4$, $\alpha_r = 20°$, $b_a = 5.08$mm, $f_t = 0.102$mm/tooth, $d = 6.87$mm)

forces distributions. In the tests, $d = 2.5$mm, $b_a = 5.08$mm, and the number of cutter flutes changes from 4 to 7. Obviously, when $m = 6$, the cutting force distribution is the best, as shown in Fig. 13(c). In this case, F_x changes from 1N to –56N during the cut-in process of each tooth, and meanwhile, $\Omega = 42.47° > \theta_m - \psi = 42.37°$, the cutting force distribution is continuous.

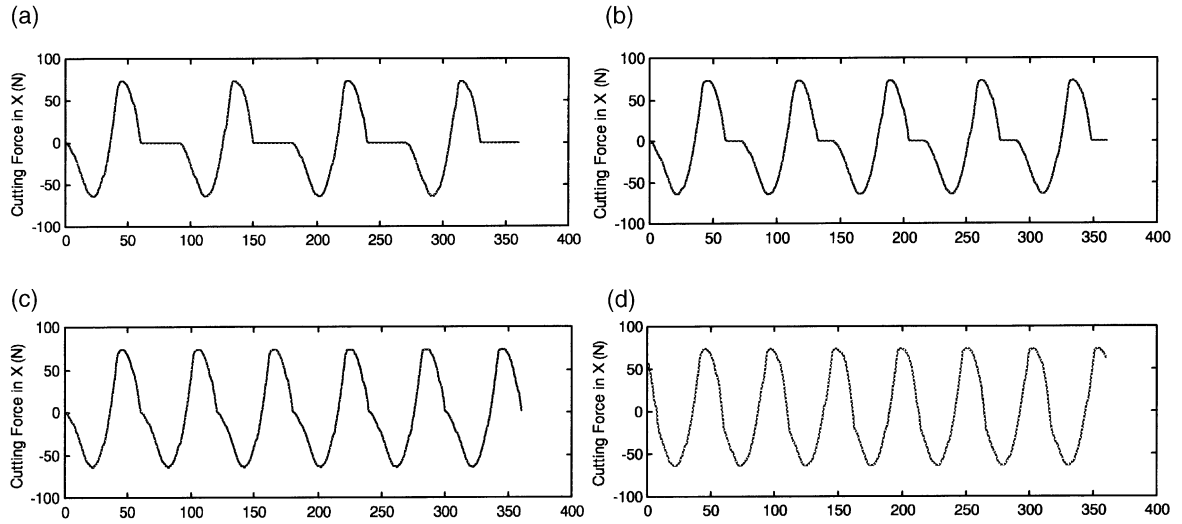

Fig. 13. Influence of number of cutter flutes on the cutting force distribution ($\alpha_r = 20°$, $b_a = 5.08$mm, $d = 2.5$mm, $f_t = 0.102$mm/tooth) (a) $m = 4$, (b) $m = 5$, (c) $m = 6$, (d) $m = 7$)

5. Conclusions and discussions

The improved theoretical dynamic cutting force model presented here reinforces the size effect of undeformed chip thickness, the influence of the effective rake angle and the flow chip flow angle in peripheral milling. Verification results indicate that the model is suitable for general peripheral milling, when the feed rate is larger than the radius of the cutting edge. For fine milling, when the feed rate is smaller than the radius of the cutting edge, the measured cutting force will be greater than the cutting force predicted by the model. This result reveals that the ploughing force is dominant in this condition and the general cutting force model is no longer effective.

Case studies reveal that the model may be very effective in reducing the surface form error due to tool deflection if the flute number, the axial depth of cut, the radial depth of cut and the feed rate are selected carefully. For some half-fine milling, both the machining productivity and quality are required to be high so the radial and axial depth of cut must be kept invariant; meanwhile, the feed rate should be kept rather high. In this case, we should select a suitable cutter with a determined flute number so as to obtain an ideal cutting force distribution. An ideal cutting force distribution means: 1) the absolute value of the cutting force component perpendicular to the feed direction during the cut-in process of each tooth is as small as possible; 2) the cutting force distribution is continuous. The two conditions ensure that the influence of the cutting force on the machining error is the smallest and the machining accuracy is the highest. The examples in Fig. 12 and Fig. 13 reveal that the productivity is kept rather high with ideal cutting force distribution. These tips are valuable for the machining of engine components and cams. With the ideal cutting force distribution, a fine milling may not be necessary and a half-fine milling may give the required precision for the machining of the parts.

Acknowledgements

This work is supported by a grant from Engineering and Physical Sciences Research Council (EPSRC). The grant number is EPSRC GR/R13395.

References

[1] Y. Altintas, P. Lee, Mechanics and dynamics of ball end milling, Transactions of the ASME: Journal of Manufacturing Science and Engineering 120 (November) (1998) 684–692.
[2] E.J.A. Armarego, R.H. Brown, The Machining of Metals, in: Prentice-Hall, New Jersey, 1969.
[3] T.S. Babin, J.M. Lee, J.W. Sutherland, S.G. Kapoor, A model for end milled surface topography, in: Proceedings of the 13th North American Metalworking Research Conference, 1985, pp. 362-368.
[4] A.E. Bayoumi, G. Yucesan, L.A. Kendall, An analytic mechanistic cutting force model for milling operations: a theory and methodology, Transactions of the ASME: Journal of Engineering for Industry 116 (August) (1994) 324–339.
[5] E. Budak, Y. Altintas, E.J.A. Armarego, Prediction of milling force coefficients from orthogonal cutting data, Transactions of the ASME: Journal of Manufacturing Science and Engineering 118 (May) (1996) 216–224.
[6] M.A. Elbestawi, F. Ismail, R. Du, B.C. Ullagaddi, Modelling machining dynamics including damping in the tool-workpiece interface, Transactions of the ASME: Journal of Engineering for Industry 116 (November) (1994) 435–439.
[7] F. Ismail, M.A. Elbestawi, R. Du, K. Urbasik, Generation of milled surface including tool dynamics and wear, Trans. Transactions of the ASME: Journal of Engineering for Industry 115 (August) (1993) 245–252.
[8] W.A. Kline, R.E. DeVor I, A. Shareef, The prediction of surface

accuracy in end milling, Transactions of the ASME: Journal of Engineering for Industry 104 (August) (1982) 272–278.
[9] F.M. Kolarits, W.R. DeVries, A mechanistic dynamic model of end milling for process controller simiulation, Transactions of the ASME: Journal of Engineering for Industry 113 (May) (1991) 176–183.
[10] D. Montgomery, Y. Altintas, Mechanism of cutting force and surface generation in dynamic milling, Transactions of the ASME: Journal of Engineering for Industry 113 (May) (1991) 160–168.
[11] T.C. Ramaraj, E. Eleftheriou, Analysis of the mechanics of machining with tapered end milling cutters, Transactions of the ASME: Journal of Engineering for Industry 116 (August) (1994) 398–404.
[12] M.C. Shaw, Metal Cutting Principles, in: Clarendon Press, Oxford, 1984.
[13] S. Smith, J. Tlusty, An overview of modeling and simulation of the milling process, Transactions of the ASME: Journal of Engineering for Industry 113 (May) (1991) 169–175.
[14] J.W. Sutherland, R.E. Devor, An improved method for cutting force and surface error prediction in flexible end milling systems, Transactions of the ASME: Journal of Engineering for Industry 108 (November) (1986) 269–279.
[15] J. Tlusty, P. Macneil, Dynamics of cutting forces in end milling, Annual of CIRP 24 (1975) 21–25.
[16] J. Tlusty, Machine dynamics, in: R.I. King (Ed.), Handbook of high-speed machining technology, Chapman and Hall, New York, 1985.
[17] J. Tlusty, Dynamics of high-speed milling, Transactions of the ASME: Journal of Engineering for Industry 108 (May) (1986) 59–67.
[18] G.B. Yucesan, Y. Altintas, Improved modelling of cutting force coefficients in peripheral milling, International Journal of Machine Tools and Manufacture 34 (4) (1994) 473–487.
[19] G.M. Zhang, S.G. Kapoor, Dynamic generation of machined surfaces, Part1: Description of a random excitation system, Transactions of the ASME: Journal of Engineering for Industry 113 (May) (1991) 137–144.
[20] G.M. Zhang, S.G. Kapoor, Dynamic generation of machined surfaces Part2: Construction of surface topography, Transactions of the ASME: Journal of Engineering for Industry 113 (May) (1991) 145–153.